Measurement of the complex transmittance of large optical elements with modulation coherent imaging

Hua Tao,[1] Suhas P. Veetil,[2] Jun Cheng,[1] Xingchen Pan,[1] Haiyan Wang,[1] Cheng Liu,[1,*] and Jianqiang Zhu[1]

[1]Shanghai Institute of Optics and Fine Mechanics, Chinese Academy of Sciences, Shanghai 201800, China

[2]Department of Engineering Technology and Science, Higher Colleges of Technology, Fujairah 1626, United Arab Emirates

*Corresponding author: chengliu@siom.ac.cn

Received 19 November 2014; revised 25 January 2015; accepted 26 January 2015; posted 29 January 2015 (Doc. ID 227149); published 26 February 2015

Accurate measurements of the transmittance of large optical elements are essential to improve the energy density in inertial confinement fusion (ICF). The required complex transmittance of such optical elements used in ICF is obtained by computing the phase difference between the illuminating and transmitting fields using modulation coherent imaging (MCI). A phase plate designed as a modulator has a known transmission function in this technique. It presents a simple and quick method to measure the transmittance of large optical elements with irregular surface profiles by retrieving it from only two diffraction patterns recorded by a CCD camera. The complex transmittance of a continuous phase plate (CPP) with a large aperture used in ICF is measured experimentally, and the results are found to agree with the designed value.

OCIS codes: (100.5070) Phase retrieval; (050.1970) Diffractive optics; (120.5050) Phase measurement; (070.0070) Fourier optics and signal processing.

http://dx.doi.org/10.1364/AO.54.001776

1. Introduction

Thousands of large-diameter optical components are employed in high-power solid-state lasers for inertial confinement fusion (ICF). Since such optical components need to carry high-power laser beams they must have excellent transmission characteristics. This in turn requires materials and systems with increasing manufacturing precisions for the production of large-diameter optical systems [1]. Inaccuracies in material uniformity or surface profile may affect the quality of the transmitted beam and eventually may lead to the failure of actual experiments [2]. So a strict control on the quality of the wavefront is required in ICF in order to focus a sufficiently high amount of energy in the region of interest [3,4].

Hartmann wavefront sensors are widely used to measure the transmittance of large-diameter optical elements to evaluate its quality while a parallel beam of light is passed through such systems [5,6]. However, since the resolution of Hartmann wavefront sensors is limited by its sub-aperture and the number of micro-lens used, the resolution obtained by such measurements is inadequate to meet the actual demand. This method is also complicated as it has much higher stability requirements and often the accuracy of the measurement is not guaranteed [7,8]. A large-aperture interferometer used in conventional interferometry usually employs a standard element in similar size as that of the element to be tested. However, obtaining such a high-precision

1559-128X/15/071776-06$15.00/0

standard component is difficult owing to its high manufacturing cost and lack of a high-quality test environment [9], thus practically making it difficult to use in the measurements of large-diameter optical components.

A phase-retrieval method called coherent diffractive imaging (CDI) was introduced based on computer iterative calculations as an alternative method to measure the phase of high-power laser beams [10]. A CDI algorithm can retrieve the complex phase directly from the diffraction pattern intensity and it seems to be a good choice for the phase measurement in the field of high-intensity lasers since it is done without using any reference beam, a standard plate, or imaging devices [11]. Later, a ptychographical iterative engine (PIE) algorithm was proposed that reconstructs the amplitude and phase of the object from a sequence of diffraction patterns, obtained by shifting the object to different distances relative to the illumination known *a priori*, to overcome the disadvantages of traditional CDI algorithms including the stagnation, low convergence, and limited field of view [12]. The modulation coherent imaging (MCI) method was proposed, which is a phase recovery algorithm developed from the PIE algorithm [13,14]. This method converges rapidly and has a less stringent dynamic range requirement on detectors that overcomes the disadvantages of PIE algorithms.

In this paper we will demonstrate that MCI method can be used to measure the complex transmittance of large-aperture elements of an ICF system. A continuous phase plate (CPP), which is a key device used for smoothing the focal spot of the high-power laser beam and having a highly irregular surface profile [15–17], is used as an example to demonstrate the feasibility of this method. It only needs to record a diffraction pattern and then the transmittance of the large-diameter component can be retrieved by certain iterative calculations that may last only a few minutes. The measured result is found to agree with the designed value.

2. Basic Principle of MCI Method

Figure 1 shows the schematic of the MCI method. It consists of an entrance plane, a modulator, and then a detector. The incident wavefront has a finite extent in the entrance plane. A constraint function of circular aperture S_n is designed for this finite extent. The modulator is a random phase plate (RPP) having a known transmission function $O(x,y)$ that is designed in order to diffract the entrance wave into a large solid angle, yielding a flattened diffraction intensity pattern. Consequently, the requirements on the dynamic range of the detector are reduced. The resulting diffraction patterns are recorded in the detector that is placed at a certain distance from the modulator. The reconstruction of the entrance wave function is done iteratively as follows, by taking a random initial guess for the entrance wave $\varphi_n(x,y)$ where n stands for the number of iterations:

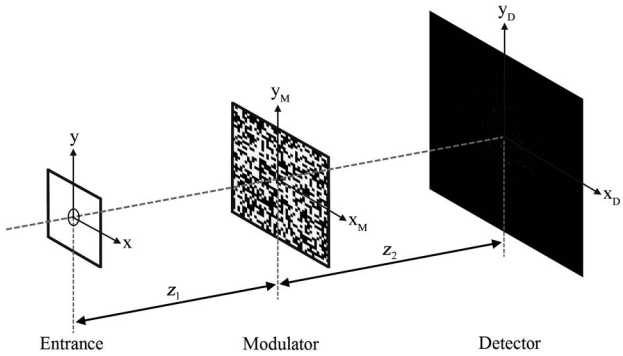

Fig. 1. Schematic of MCI method. Three planes are defined in this configuration.

1. Given the constraint function of circular aperture $S_n = \begin{cases} 1, & 0 \le r \le r_n \\ 0, & r > r_n \end{cases}$ for the entrance plane, where r is the radius of the circular aperture, and r_n $(n = 1)$ initially is a small constant of the order of microns. The exit wave function at the entrance plane is $\varphi_{e,n}(x,y) = \varphi_n(x,y) \cdot S_n$, where n represents the nth iteration.

2. Propagate $\varphi_{e,n}$ to the modulator plane, the entrance wave function at modulator plane is $P_{m,n}(x,y) = \mathrm{FFT}[\varphi_{e,n}(x,y), z_1]$, in terms of the fast Fourier-transform (FFT) operator.

3. The exit wave function at the modulator plane is $\varphi_{m,n}(x,y) = P_{m,n}(x,y) \cdot O(x,y)$, where $O(x,y)$ is the transmittance function of the designed RPP.

4. Propagate the exit wave function to the detector plane. The wave function at detector plane is $\phi_{m,n}(x,y) = \mathrm{FFT}[\varphi_{m,n}(x,y), z_2]$, where FFT represents Fourier propagation to a distance z_2 in the nth iteration.

5. Replace the amplitude of the wave function obtained in Step 4 with the diffraction pattern intensity recorded by the CCD. The corrected wave function is now represented by $\phi_{c,n}(x,y) = \sqrt{I}\exp[i \arg |\phi_{m,n}(x,y)|]$, where I is the intensity of diffraction patterns recorded by the CCD, and $\arg|\phi_{m,n}(x,y)|$ represents the phase of $\phi_{m,n}(x,y)$.

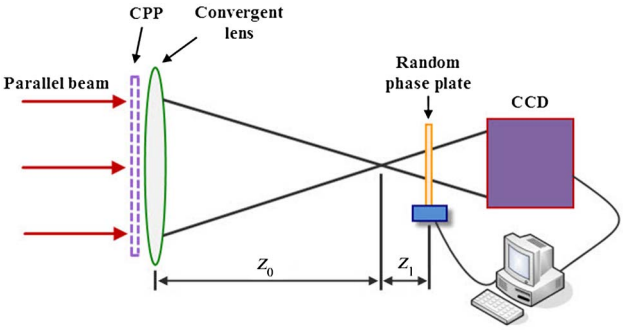

Fig. 2. Experimental setup for measuring the transmission functions with MCI. Parallel beam focused by a nonspherical lens illuminates the test element, which is a CPP and then an RPP near the focal plane. Resulting diffraction patterns are recorded by a CCD.

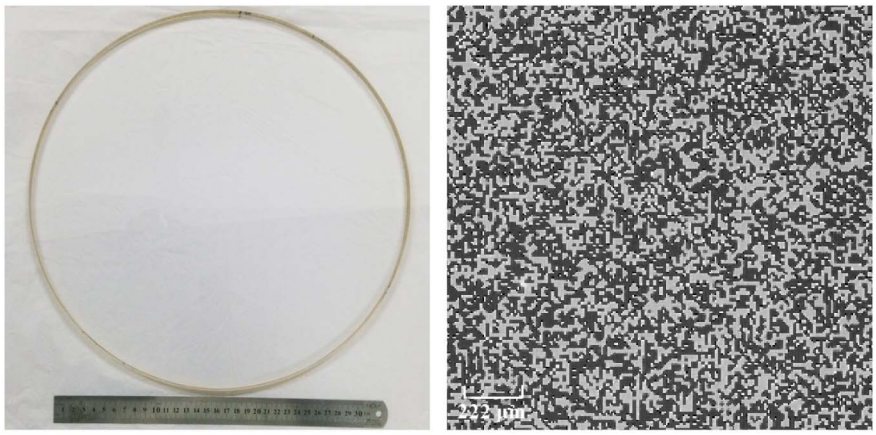

(a) (b)

Fig. 3. (a) CPP used in the work. Diameter is shown to be 31 cm; (b) phase distribution $O(x,y)$ of the RPP obtained with the ePIE algorithm.

6. The wave function at the back side of the modulation plane is obtained as $\varphi_{c,n}(x,y) = \mathrm{FFT}^{-1}[\phi_{c,n}(x,y),z_2]$, where $\mathrm{FFT}^{-1}[\phi_{c,n}(x,y),z_2]$ represents Fourier back-propagation to a distance z_2 in the nth iteration.

7. Update the function

$$P_{\mathrm{new}}(x,y) = P_{m,n}(x,y) + \frac{|O(x,y)|}{|O(x,y)|_{\max}} \frac{O(x,y)^*}{[|O(x,y)|^2 + \alpha]} \times [\varphi_{c,n}(x,y) - P_{m,n}(x,y) \cdot O(x,y)],$$

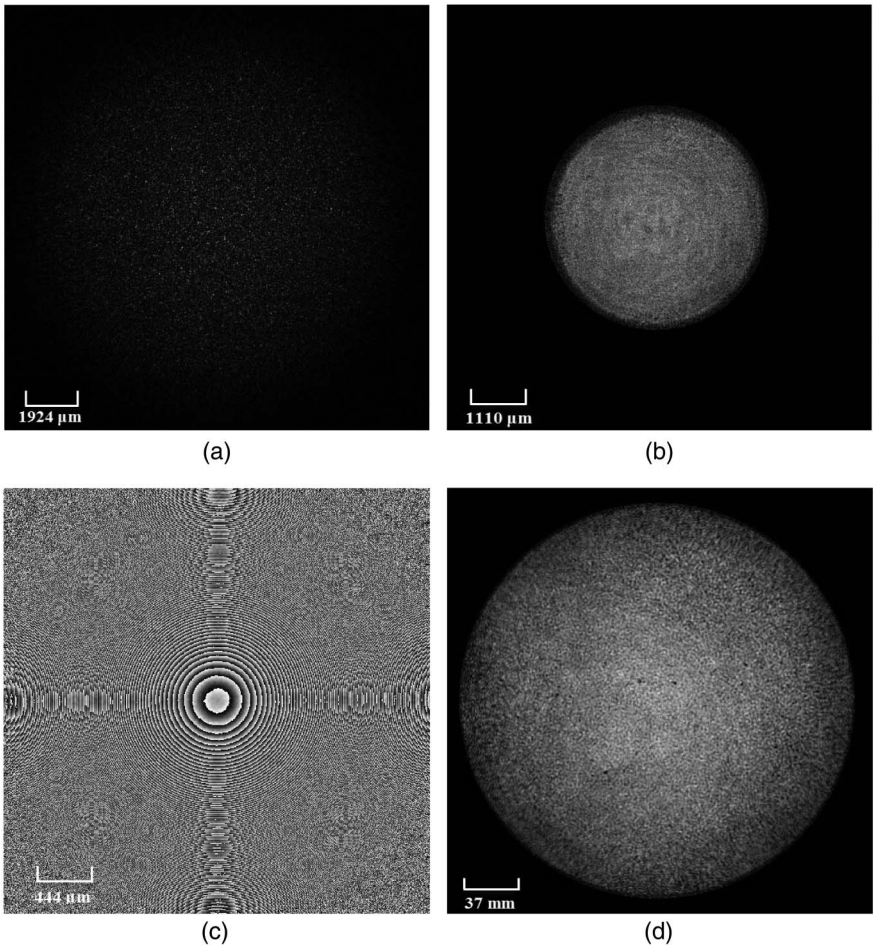

(a) (b) (c) (d)

Fig. 4. (a) Diffraction patterns recorded by CCD without CPP; (b) corresponding reconstructed modulus of illumination on the RPP; (c) corresponding reconstructed phase distribution of illumination on the RPP; (d) numerically obtained amplitude distribution $U(x',y')$ before the condenser lens.

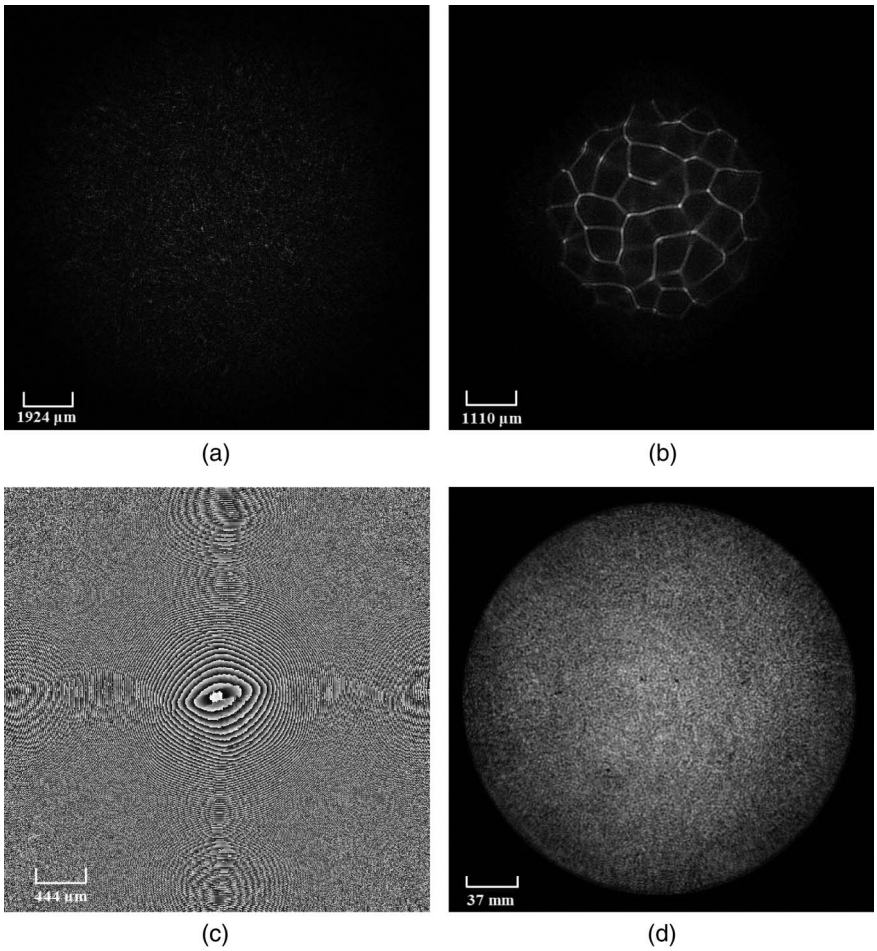

Fig. 5. Recorded diffraction pattern and reconstructed results with CPP and RPP along the light path; (a) diffraction pattern recorded by CCD; (b) reconstructed amplitude of illumination on the RPP; (c) reconstructed phase distribution of illumination on the RPP; (d) numerically obtained amplitude distribution $T(x',y')$ before the condenser lens.

where α is an appropriately chosen constant to suppress the noise [12].

8. Propagate $P_{\text{new}}(x,y)$ to the entrance plane, the exit wave function at the entrance plane is $\varphi'_{e,n}(x,y) = \text{FFT}^{-1}[P_{\text{new}}(x,y),z_1]$, where $\text{FFT}^{-1}[P_{\text{new}}(x,y),z_1]$ represents Fourier back-propagation to a distance z_1 in the nth iteration.

9. Increase the value r_{n+1} about 0.1 μm in each iteration, update the exit wave function at entrance plane as $\varphi_{e,n+1}(x,y) = \varphi'_{e,n}(x,y) \cdot S_{n+1}$.

10. Repeat Steps 1–9 until the change between two successive iterations of the entrance wave $\varphi_{e,n}(x,y)$ becomes sufficiently small. The iteration is stopped in this case and the final wave functions obtained, $\varphi_n(x,y)$ and $P_{m,n}(x,y)$, are accurate distributions of the light field at the entrance and at the modulator plane. $P_{m,n}(x,y)$ is obtained as $P_{m,n}(x,y) = \text{FFT}[\varphi_{e,n}(x,y),z_1]$.

3. Complex Transmittance of Large Optical Elements with MCI

The large optical element to be studied is taken to be a CPP, which has a highly irregular surface profile. It is used as a key element of the ICF system for smoothing the laser beam of the ICF system to ensure an ideal focal spot. A small departure in its surface profile from its designed shape can drastically increase the electrical field in some place and increase the risk of radiation damage in the frequency-doubling crystal, focus lens, sample grating, and so on.

The experimental setup for measuring the transmittance of a large-aperture optical element with MCI method is schematically shown in Fig. 2. A parallel beam of 28 cm diameter first passes through the CPP and then focused by an aspheric condense lens with a focal length of 1575 mm. It then illuminates a RPP kept near the focal plane. The focal plane is equivalent to the entrance plane defined in Fig. 1 in this work. The phase plate consists of an array of pixels that randomly take values of either 0 or π with the same probability. A computer is used for recording the diffraction pattern and a translation stage control is used as the PIE algorithm is applied to accurately measure the transmittance function $O(x,y)$ of the designed RPP. A diffraction pattern is recorded by the CCD camera behind the RPP. The illuminating field on the RPP plane $P'_{m,n}(x,y)$ is then obtained from this diffraction pattern using the MCI method. The test element is then removed

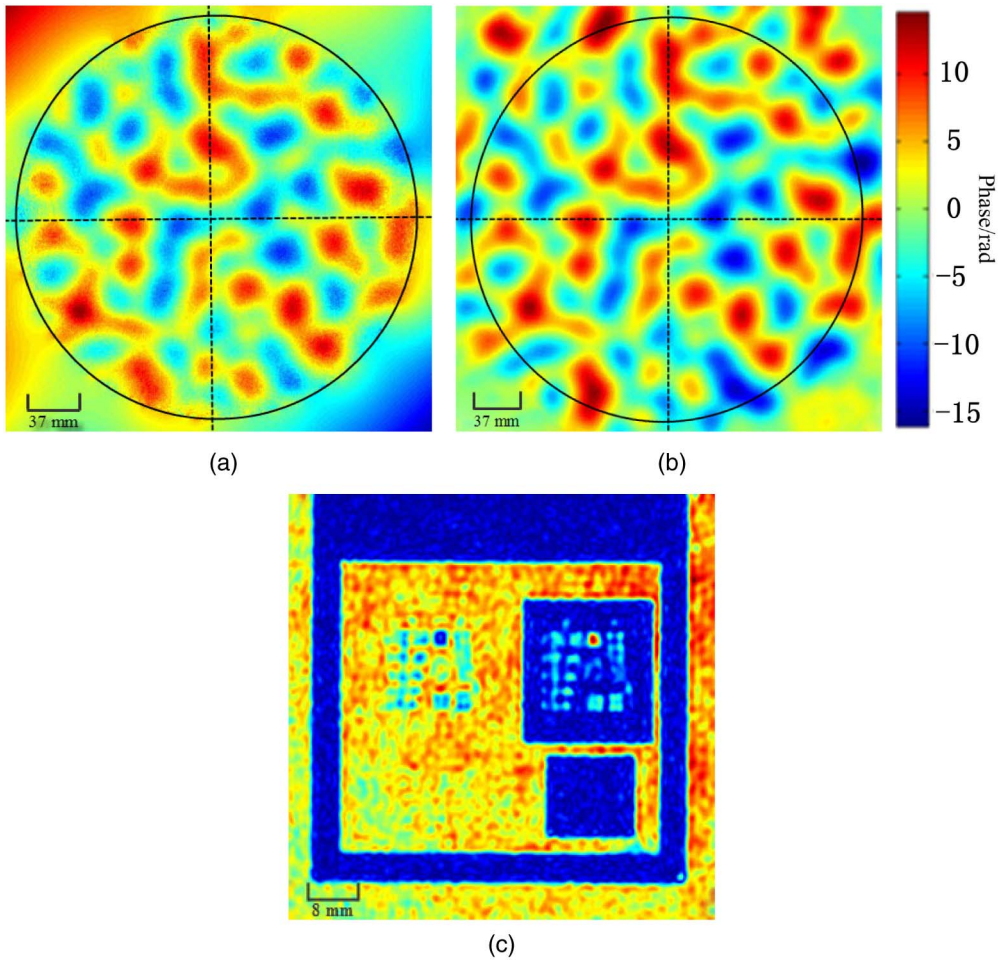

Fig. 6. (a) Phase distribution of the CPP obtained by the MCI method; (b) phase distribution used in the design of the CPP; (c) measured transmittance distribution of a USAF 1951 target.

and another diffraction pattern is recorded by the CCD camera. The resulting illuminating field on the RPP plane $P_{m,n}(x,y)$ is also obtained from this diffraction pattern with the same MCI method.

We can now obtain the illuminating field $U(x',y')$, which falls on the optical element being studied, and the transmitting field $T(x',y')$, which is leaving the optical element by numerically propagating the reconstructed wave functions present at the modulator plane, $P_{m,n}(x,y)$ and $P'_{m,n}(x,y)$, to the plane exactly behind the condenser lens using the following Fresnel diffraction formula

$$U(x',y') = \frac{\exp(ikz)}{i\lambda z}\iint P_{m,n}(x,y) \times \exp\left[ik\frac{(x'-x)^2+(y'-y)^2}{2z}\right]\mathrm{d}x\mathrm{d}y, \quad (1)$$

$$T(x',y') = \frac{\exp(ikz)}{i\lambda z}\iint P'_{m,n}(x,y) \times \exp\left[ik\frac{(x'-x)^2+(y'-y)^2}{2z}\right]\mathrm{d}x\mathrm{d}y; \quad k = 2\pi/\lambda, \quad (2)$$

where λ is the wavelength of the parallel beam, and z is the propagation distance. The complex transmittance of the optical element studied can be obtained by calculating the phase of $U(x',y')T^*(x',y')$, where $T^*(x',y')$ is the conjugate of $T(x',y')$. The wavelength of the laser source used is 632.8 nm, and the CCD used is PIKE-421B (Allied Vision Technologies, AVT).

Figure 3(a) shows the manufactured CPP plate, which has a highly irregular surface profile and having a diameter of 31 cm. Figure 3(b) shows the measured phase distribution of the RPP with the ePIE algorithm. The phase distribution is either zero or π represented in gray or black in Fig. 3. Each cell size of the phase distribution is 7.4 μm × 7.4 μm and it is randomly distributed. This can effectively disperse the incident light beam and hence the dynamic range requirement of the detector is reduced.

The diffraction pattern obtained with only RPP along the light path is shown in Fig. 4(a), where the obvious speckle is due to the random structure of the RPP. With the MCI algorithm, the illumination on the modulator plane is reconstructed. Figures 4(b) and 4(c) show the reconstructed modulus and phase, respectively. By propagating this numerically reconstructed field to the plane exactly behind the

condenser lens, the amplitude and the phase of the illuminating field $U(x',y')$ is generated. Figure 4(d) shows the amplitude of $U(x',y')$.

The results obtained by repeating the previously mentioned steps with the CPP placed before the condenser lens are shown in Fig. 5. The detection and reconstruction procedures are repeated to numerically obtain the transmitting field $T(x',y')$. The recorded diffraction pattern is shown in Fig. 5(a), and the amplitude and phase of the $P'_{m,n}(x,y)$ are shown in Figs. 5(b) and 5(c), respectively. By propagating $P'_{m,n}(x,y)$ to the back plane of the CPP we obtain the transmitting function $T(x',y')$, whose amplitude distribution is shown in Fig. 5(d).

The phase modulation of the CPP obtained by the proposed method is shown within the circle in Fig. 6(a). Figure 6(b) is the phase distribution designed initially for the surface profile of CPP that would generate the required focal spot in ICF system. We can find that the surface profile of the CPP is highly irregular with values ranging from 13.8714 to −15.4880 rad. While commonly used techniques have their limitations on the measurements of transmittance, the proposed MCI method can quickly obtain the transmittance measurements that are comparable to that of the design values of the CPP. The achievable resolution of the transmittance of the CPP retrieved by the outlined MCI method is demonstrated by placing a United States Air Force (USAF) 1951 target before the condenser lens. The transmittance obtained is shown in Fig. 6(c) and clearly shows a resolution that is about 2 mm. It is a satisfactory result in cases involving such large optical elements.

4. Conclusion

The MCI technique is applied to obtain the complex transmittance of large-aperture optical elements of an ICF system. This can be extended to optical systems with several large-aperture elements for which transmittance are not directly measurable using most of the commonly used techniques. The feasibility of the proposed method is demonstrated using a CPP plate as an example, which is a key optical element in a high-energy laser facility. To our knowledge, this is the first time that the MCI technique is used for measuring the complex transmittance of large optical elements.

This work is supported by Grant 29201431151100301 and One Hundred Person Project of the Chinese Academy of Sciences, China (Grant No. 902012312D1100101).

References

1. D. J. Trummer, R. J. Foley, and G. S. Shaw, "Stability of optical elements in the NIF target area building," Proc. SPIE **3492**, 363–371 (1999).
2. W. H. Williams, J. M. Auerbach, M. A. Henesian, J. K. Lawson, J. T. Hunt, R. A. Sacks, and C. C. Widmayer, "Modeling characterization of the National Ignition Facility focal spot," Proc. SPIE **3264**, 93–104 (1998).
3. C. R. Wolfe and J. K. Lawson, "The measurement and analysis of wavefront structure from large aperture ICF optics," Proc. SPIE **2633**, 361–385 (1995).
4. H. Wang, C. Liu, X. He, X. Pan, S. Zhou, R. Wu, and J. Zhu, "Wavefront measurement techniques used in high power lasers," High Power Laser Sci. Eng. **2**, e25 (2014).
5. W. Jiang and H. Li, "Hartmann–Shack wavefront sensing and control algorithm," Proc. SPIE **1271**, 82–93 (1990).
6. G. Cao and X. Yu, "Accuracy analysis of a Hartmann–Shack wavefront sensor operated with a faint object," Opt. Eng. **33**, 2331–2335 (1994).
7. V. Y. Zavalova and A. V. Kudryashov, "Shack–Hartmann wave-front sensor for laser beam analyses," Proc. SPIE **4493**, 277–284 (2002).
8. S. Sato, T. Mori, Y. Higashi, S. Haya, M. Otsuka, and H. Yamamoto, "A profilometer for synchrotron radiation mirrors," J. Electron Spectrosc. Relat. Phenom. **80**, 481–484 (1996).
9. X. Liu, Y. Gao, and M. Chang, "A partial differential equation algorithm for wavefront reconstruction in lateral shearing interferometry," J. Opt. A **11**, 045702 (2009).
10. S. Matsuoka and K. Yamakawa, "Wave-front measurements of terawatt-class ultrashort laser pulses by the Fresnel phase-retrieval method," J. Opt. Soc. Am. B **17**, 663–667 (2000).
11. X. Pan, S. P. Veetil, C. Liu, Q. Lin, and J. Zhu, "High-contrast imaging for weakly diffracting specimens in coherent diffraction imaging," Chin. Opt. Lett. **11**, 021103 (2013).
12. J. M. Rodenburg and H. M. Faulkner, "A phase retrieval algorithm for shifting illumination," Appl. Phys. Lett. **85**, 4795–4797 (2004).
13. F. Zhang and J. M. Rodenburg, "Phase retrieval based on wave-front relay and modulation," Phys. Rev. B **82**, 121104 (2010).
14. F. Zhang, I. Peterson, J. Vila-Comamala, A. Diaz, F. Berenguer, R. Bean, B. Chen, A. Menzel, I. K. Robinson, and J. M. Rodenburg, "Translation position determination in ptychographic coherent diffraction imaging," Opt. Express **21**, 13592–13606 (2013).
15. H. Wang, C. Liu, S. P. Veetil, X. Pan, and J. Zhu, "Measurement of the complex transmittance of large optical elements with ptychographical iterative engine," Opt. Express **22**, 2159–2166 (2014).
16. C. A. Haynam, P. J. Wegner, J. M. Auerbach, M. W. Bowers, S. N. Dixit, G. V. Erbert, G. M. Heestand, M. A. Henesian, M. R. Hermann, K. S. Jancaitis, K. R. Manes, C. D. Marshall, N. C. Mehta, J. Menapace, E. Moses, J. R. Murray, M. C. Nostrand, C. D. Orth, R. Patterson, R. A. Sacks, M. J. Shaw, M. Spaeth, S. B. Sutton, W. H. Williams, C. C. Widmayer, R. K. White, S. T. Yang, and B. M. VanWonterghem, "National Ignition Facility laser performance status," Appl. Opt. **46**, 3276–3303 (2007).
17. J. Néauport, X. Ribeyre, J. Daurios, D. Valla, M. Lavergne, V. Beau, and L. Videau, "Design and optical characterization of a large continuous phase plate for laser integration line and laser megajoule facilities," Appl. Opt. **42**, 2377–2382 (2003).